The Journal of Experimental Biology 213, 3269-3279

doi:10.1242/jeb.046052

Aerodynamic characteristics of flying fish in gliding flight

Hyungmin Park and Haecheon Choi*

School of Mechanical and Aerospace Engineering, Seoul National University, Seoul, 151-744, Korea and
Institute of Advanced Machinery and Design, Seoul National University, Seoul, 151-744, Korea

*Author for correspondence (choi@snu.ac.kr)

Accepted 17 June 2010

SUMMARY

The flying fish (family Exocoetidae) is an exceptional marine flying vertebrate, utilizing the advantages of moving in two different media, i.e. swimming in water and flying in air. Despite some physical limitations by moving in both water and air, the flying fish has evolved to have good aerodynamic designs (such as the hypertrophied fins and cylindrical body with a ventrally flattened surface) for proficient gliding flight. Hence, the morphological and behavioral adaptations of flying fish to aerial locomotion have attracted great interest from various fields including biology and aerodynamics. Several aspects of the flight of flying fish have been determined or conjectured from previous field observations and measurements of morphometric parameters. However, the detailed measurement of wing performance associated with its morphometry for identifying the characteristics of flight in flying fish has not been performed yet. Therefore, in the present study, we directly measure the aerodynamic forces and moment on darkedged-wing flying fish (*Cypselurus hiraii*) models and correlated them with morphological characteristics of wing (fin). The model configurations considered are: (1) both the pectoral and pelvic fins spread out, (2) only the pectoral fins spread with the pelvic fins folded, and (3) both fins folded. The role of the pelvic fins was found to increase the lift force and lift-to-drag ratio, which is confirmed by the jet-like flow structure existing between the pectoral and pelvic fins. With both the pectoral and pelvic fins spread, the longitudinal static stability is also more enhanced than that with the pelvic fins folded. For cases 1 and 2, the lift-to-drag ratio was maximum at attack angles of around 0 deg, where the attack angle is the angle between the longitudinal body axis and the flying direction. The lift coefficient is largest at attack angles around 30~35 deg, at which the flying fish is observed to emerge from the sea surface. From glide polar, we find that the gliding performance of flying fish is comparable to those of bird wings such as the hawk, petrel and wood duck. However, the induced drag by strong wing-tip vortices is one of the dominant drag components. Finally, we examine ground effect on the aerodynamic forces of the gliding flying fish and find that the flying fish achieves the reduction of drag and increase of lift-to-drag ratio by flying close to the sea surface.

Key words: flying fish, gliding, wing morphology, lift, drag, stability, ground effect.

INTRODUCTION

The flying fish (family Exocoetidae) is an exceptional marine flying vertebrate showing successful gliding capabilities in air (Hertel, 1966; Rayner, 1986; Vogel, 1994). The flying fish glides over a total distance of as much as 400 m in 30 s by a successive sequence of taxiing and flight, and its maximum flight speed is in the region of 10~20 m s^{-1} (Hertel, 1966; Fish, 1990; Davenport, 1994). Morphologically, pairs of fins are physically modified to function as wings for flight and some genera such as *Cypsilurus* have a body with flattened bottom to generate additional lift (Breder, 1930; Davenport, 1992; Davenport, 1994). The flying fish's morphological and behavioral adaptations for its excellent gliding-flight capability have been examined, and several aspects (e.g. flight pattern of gliding and taxiing, the relationship between wing loading and aspect ratio of the pectoral fins, and possible importance of ground effect) of its flight have been determined or conjectured (Davenport, 1994).

Although reasons for the flight of flying fish have been suggested (i.e. escape from underwater predators or saving of transport cost) (Rayner, 1986; Davenport, 1994), the exact reason is still not clear. Nevertheless, their behavioral adaptation for flight is quite unique. When they emerge from the sea or the gliding speed decreases at the end of one glide, some flying fish dip the lower lobe of the caudal fin and beat the tail, which is called taxiing (Hertel, 1966; Fish, 1990; Davenport, 1992; Davenport, 1994). Supported by the wings (stretched pectoral fins), they use this taxiing to gain additional speed for successive gliding flights (Breder, 1930; Mills, 1936a; Mills, 1936b). The glide trajectory of flying fish has been observed to be almost straight (i.e. parallel to the sea surface) and its gliding height is an order of full span of the pectoral fins (Latimer-Needham, 1951; Hertel, 1966; Fish, 1991; Kawachi et al., 1993). Kawachi et al. (Kawachi et al., 1993) analyzed the gliding path of flying fish, using a simple analytical method based on the energy balance and an optimal control theory, to evaluate the gliding strategies for maximum gliding distance and time, respectively. They found that its straight gliding path is for maximum gliding distance, rather than for the longest gliding time.

As mentioned above, from the field observations and measurements of morphometric parameters, several features of flying-fish flight have been determined. However, detailed data on the wing performance are required to identify the flight capability of flying fish. Hence, in the present study, we investigated the wing performance of flying fish by directly measuring the aerodynamic forces, moment and conducting flow visualizations in a wind tunnel. We also examined how the flight performance is affected by the wing morphology and compared it with those of other flying animals. Finally, we examined the effect of water and solid surfaces underneath the flying fish model in a wind tunnel, and measured the aerodynamic forces and performed flow visualization to study the ground effect.

MATERIALS AND METHODS

Flying-fish models

About 40 darkedged-wing flying fish (*Cypselurus hiraii*, Abe) were caught in the East Sea of Korea in cooperation with the National Federation of Fisheries Cooperatives of Korea. The flying fish were then separately wrapped in a plastic bag in a fresh state and then all of them were put in an icebox, during which they were put down naturally. Five fish of similar sizes were selected and stuffed in the appropriate gliding positions (see below) at the Korea Research Center of Maritime Animals. These five models of flying fish are used in our experiment. The flying fish were stuffed within a day after they were captured. During the preparation of our fish models, they were neither frozen nor preserved in alcohol. Before stuffing the flying fish, the body mass, wing lengths and overall three-dimensional body geometry of each fish were measured, and these properties were conserved during the stuffing procedure as far as possible. To maintain the geometries of wings and body, the wings were fully spread and fixed, and urethane foam was injected inside the body.

The flying fish can be classified into two categories depending on the wing configuration. One is the 'four-winger' (Davenport, 1992; 1994) or 'biplane-type' (Breder, 1930; Fish, 1990), where both pectoral and pelvic fins are hypertrophied (e.g. *Cypsilurus*). The other is the 'two-winger' or 'monoplane-type', in which only the pectoral fins are enlarged (e.g. *Exocoetus*). *Cypselurus hiraii* belongs to the 'four-winger' or 'biplane-type' category.

To investigate the effect of wing morphology on the aerodynamic performance of flying fish, wing–body configurations of the five model fish were chosen as follows (Fig. 1): (1) both the pectoral and pelvic fins spread (models L_1–L_3); (2) only pectoral fins spread with pelvic fins folded against the body (model M); (3) body only with both the pectoral and pelvic fins folded (model N). Furthermore, we varied the lateral dihedral angle of the pectoral fins for models L_1–L_3 to determine how it affects the aerodynamic performance. The wings of flying fish are composed of soft membrane supported by fin rays. Their leading edge is stiff but the trailing edge is flexible. All the fin rays are located on the lower wing surface, so the upper wing surface is smooth and the lower surface is ribbed. In the present study, the wing shape of each model was determined by fully spreading out the flying fish fin. Because the dried fin is weak and easily torn, we attached a very thin nylon cloth to the upper fin surface. For each model, we measured the morphometric parameters that are defined in Fig. 2.

Force and moment measurements

Force and moment measurements were conducted in an open-circuit blowing-type wind tunnel. Fig. 3 shows a schematic diagram of the flying-fish model in the wind tunnel. x, y and z denote the streamwise, vertical and spanwise directions, respectively, and the origin is located at the center of gravity of the flying-fish model (near the trailing edge of the pectoral fins in the streamwise direction). The test section was made of acryl and measured 3 m×0.3 m×0.6 m in the streamwise, vertical and spanwise directions, respectively. The maximum wind speed at the test section was 30 m s^{-1}, and the uniformity of the mean velocity and background turbulence intensity were both within 0.5% at 12 m s^{-1}. The aerodynamic force and moment on the fish model were measured with a six-axis force/torque sensor (NANO17, ATI Industrial Automation, Inc., Apex, NC, USA). The resolutions of the sensor in measuring the force and moment are 1/1280 N and 1/256 Nmm, respectively. From the weight test, we found that the sensor showed an excellent linearity (±1%) in the range of interest.

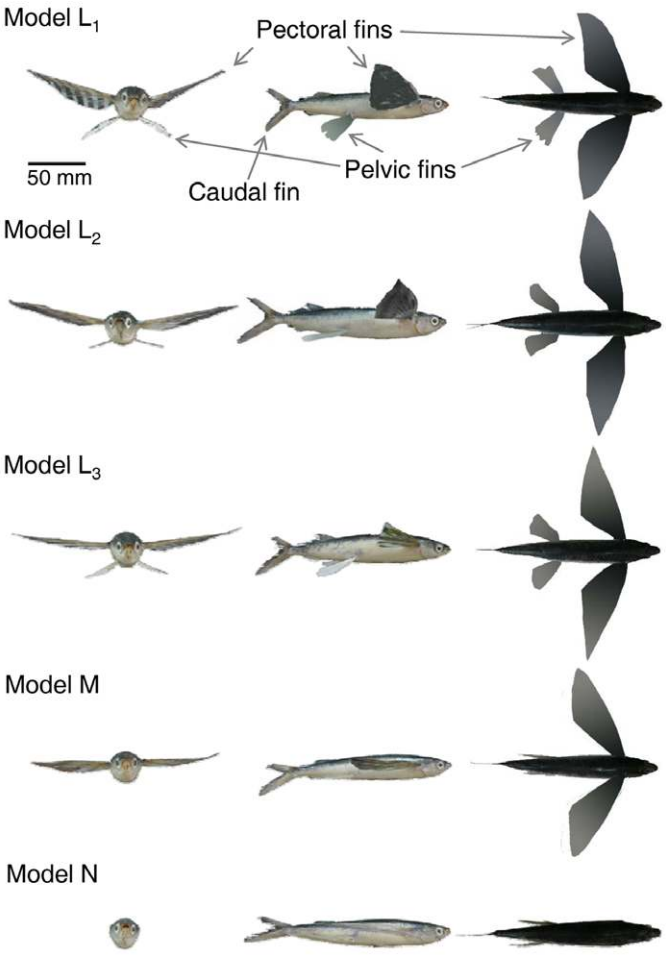

Fig. 1. Front (left), side (middle) and plan (right) views of the flying-fish models used in the present study. These models were stuffed darkedged-wing flying fish (*Cypselurus hiraii*).

A slender strut was assembled on the lower surface of the fish model at a streamwise location near the trailing edge of the pectoral fins and was directly mounted on the force/torque sensor. To minimize the effect of strut, its cross-sectional shape was chosen to be a slender ellipse with a ratio of major to minor axis of 3.36. The height of the strut was adjusted to locate the flying-fish model at the center of the test section. Varying the attack angle (α; angle between the longitudinal body axis and the free-stream direction; Fig. 2) from –15 deg to 45 deg by increments of 5 deg, we simultaneously measured the lift, drag and pitching moment. The angle of attack was controlled by an in-house device equipped with a revolving stage which had a resolution of 1 deg of rotation. The signals from the force/torque sensor were digitized by an A/D converter (PXI-6259, National Instruments Co., Austin, TX, USA) and sampled for 300 s at the rate of 10 kHz to obtain a fully converged mean value. The voltage outputs from the sensor were calibrated using the calibration matrix supplied with the sensor. The forces and moment were measured five times for each fish model and the averaged values are reported. The repeatability errors of force and moment measurements were within ±1.5%. The lift, drag and pitching moment on the struts alone were separately measured and used for the correction of those measured with each model. The measurements were performed at the free-stream velocity (u_∞) of 12 m s^{-1}, the corresponding Reynolds number of which, based on

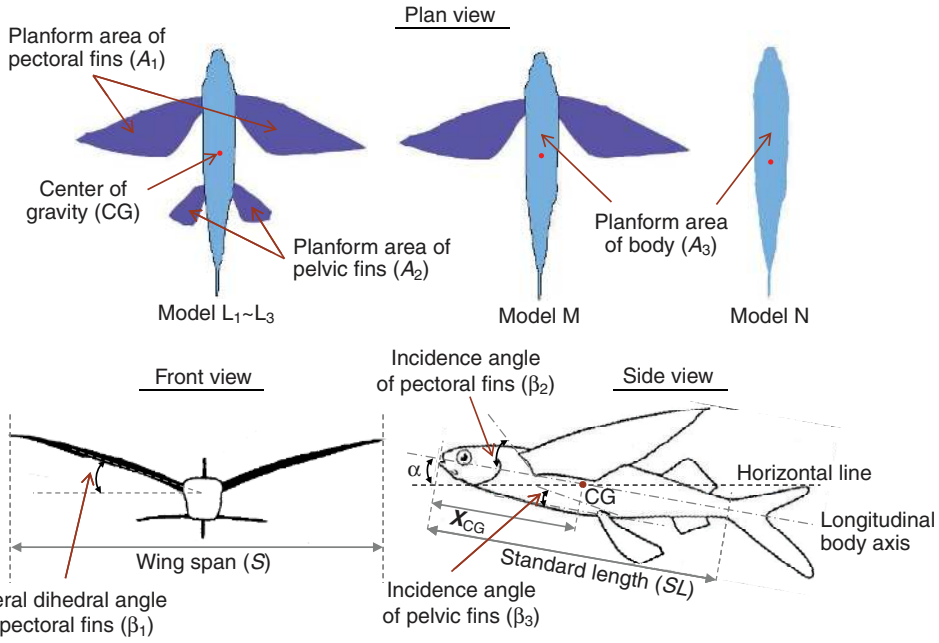

Fig. 2. Definitions of the morphometric parameters.

the average wing chord length (c) of pectoral fin, is Re=1.9–2.2×10^4, depending on the model. This meets the typical condition of gliding flight of real flying fish (Hertel, 1966; Rayner, 1986; Fish, 1990; Davenport, 1994).

Ground effect

To examine the aerodynamic performance of flying-fish flight in ground effect, we considered two kinds of ground, i.e. solid and water surfaces. To provide a water surface beneath the flying-fish model, we eliminated a part of the bottom wall of the test section [0.4 m (x)×0.5 m (z)] and installed a tank in its place. This was filled with water to just below the bottom wall of the test section to avoid any overflow. For each ground condition, we measured the drag and lift forces on the models L_3 and N at the attack angle (α) of 0 deg by varying the flight height (h), i.e. the distance between the ground and the lower surface of the body. Owing to the slight inconsistency of the water surface, the non-dimensional height r=h/(S/2)=0.33 is the closest distance between the body and water surface (r=0.21 for a solid surface).

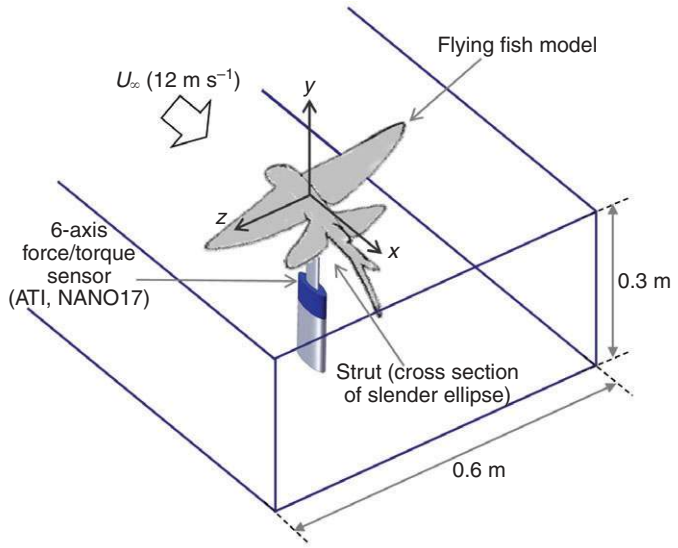

Fig. 3. Schematic diagram of the experimental setup.

Flow visualization

To investigate the flow structure around a gliding flying fish and identify the sources of its aerodynamic performance, we performed a smoke-wire flow visualization. For flow visualization, we focused on the model L_3, which showed the best aerodynamic performance of the five flying-fish models considered (see below). The flow visualizations were performed at u_∞=6 m s^{-1} for a clear representation of flow structures and the corresponding Re was ≈10^4. We installed a smoke wire in front of the leading edge of the pectoral fins and observed the streamwise flow structure (side view) at z/S=0, 0.1, 0.18 and 0.49, respectively, where S is the full span of the pectoral fins (see Fig. 2). We varied the attack angle α at 0 deg, 10 deg, 20 deg and 30 deg. The RP-1 fog fluid from Red Point Inc. (McAllen, TX, USA) and a 6 W argon laser (Stabilite 2017; Spectra-Physics, Santa Clara, CA, USA) with modulator (N30210) were used for the smoke-generating material and light source, respectively. The triggering of the smoke-line generation, digital camera (10D) and laser operation were synchronized *via* an A/D converter (PXI-6259; National Instruments Co.). We also used an array of smoke wires (14 vertical nichrome wires of the diameter of 0.2 mm connected to multiple 30 V DC power supplies and solid state relays) to observe the cross-plane flow structure (end view) in the wake behind a flying fish. We investigated the modification of the wake structure behind a flying fish in ground effect by varying the flight height r (=0.33, 0.67 and 1.12, respectively).

RESULTS AND DISCUSSION

Morphometrics

Table 1 shows the morphometric parameters measured for five flying-fish models. Definitions of these parameters are shown in Fig. 2. It is known that the adult flying fish are of variable size (150~500 mm maximum standard length) (Davenport, 1994) and the standard lengths (SL) of the present models are about 200 mm. The pectoral fins are slightly swept back as shown in Fig. 1 and

Table 1. Morphometric parameters for the darkedged-wing flying fish (*Cypselurus hiraii*) models

Model*	L_1	L_2	L_3	M	N
Standard length, *SL* (mm)	205	209	203	199	202
Body mass, *W* (kg)	0.06	0.05	0.06	0.04	0.04
Wing area of pectoral fins A_1 (mm^2)	7069	6997	6377	5498	0
Wing area of pelvic fins A_2 (mm^2)	1603	1745	1837	0	0
Planform area of body A_3 (mm^2)	4377	4501	4474	4258	4640
Wing span†, *S* (mm)	252	260	261	233	–
Aspect ratio†, AR ($=S^2/A_1$)	9.0	9.7	10.7	9.9	–
Average wing chord length†, *c* (mm)	28	27	24	24	–
Dihedral angle of pectoral fin, β_1 (deg)	22	12	7	5	–
Incidence angle of pectoral fin, β_2 (deg)	12	15	12	8	–
Incidence angle of pelvic fin, β_3 (deg)	2	2	5	–	–
Location of center of gravity, x_{CG}/SL	0.39	0.43	0.42	0.44	0.47

*Graphical representation of each parameter is shown in Fig. 2.
†Aspect ratio, wing span and averaged chord length are based on the pectoral fins only.

have an aspect ratio of 9.0~10.7, which is comparable to those of birds (Withers, 1981; Fish, 1990; Vogel, 1994). In the process of stuffing the flying fish, the lateral dihedral angles (β_1) of the pectoral fins were artificially modified to be 22 deg, 12 deg and 7 deg for models L_1, L_2 and L_3, respectively, but other parameters were kept close to the natural state. Similar to the wings of modern aircraft that have the positive incidence angle of several degrees, the pectoral and pelvic fins of flying fish also have positive incidence angles (β_2 and β_3) from the longitudinal body axis (Fig. 2). In the present models, the incidence angles of pectoral and pelvic fins were 8~15 deg and 2~5 deg, respectively. It has been suggested that the flying fish controls these angles according to the flight conditions (Hubbs, 1933), but the ranges of the incidence angle during real gliding flight are not available in the literature. We found only one illustrative diagram (Breder, 1930) in which the incidence angles of pectoral and pelvic fins are shown to be 17 deg and 3 deg, respectively.

Fig. 4 shows the allometric relationship between the wing loading and standard length of our fish models (L_1, L_2 and L_3), together with those from Fish (Fish, 1990) and Davenport (Davenport, 1992).

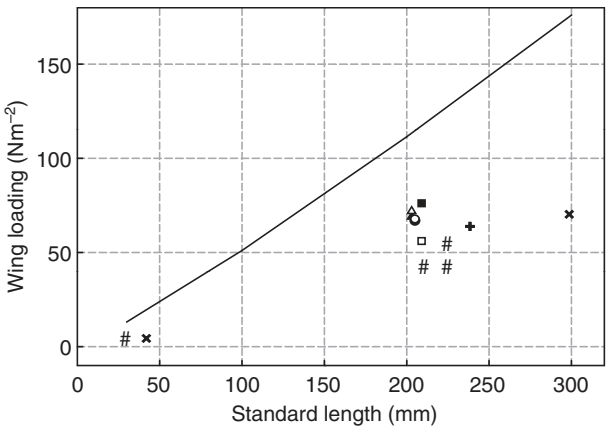

Fig. 4. Relationship between the wing loading and standard length. *Cypselurus hiraii* (present study; open circle and solid circle, model L_1; open square and closed square, model L_2; open triangle and closed triangle, model L_3; open symbols are from the direct measurement of the body weight and solid ones are from the direct measurement of lift force in wind tunnel experiments); *Hirundichthys affinis* [# (Davenport, 1992)]; *Cypsilurus cyanopterus* [× (Davenport, 1992)]; *Cypsilurus heterurus* [+ (Davenport, 1992)]; *Cypselurus* [solid line (Fish, 1990)].

For this figure, our wing-loading data were obtained in two different ways: one is the fish body mass, measured directly before stuffing, and the other is the lift force measured directly from our wind tunnel experiment at the attack angle of 0 deg. The reason why the attack angle of 0 deg was chosen is given later in this paper. As shown in Fig. 4, the two data are nearly same for models L_1 and L_3, but shows about 30% deviation for model L_2. Overall, our data are close to those of Davenport (Davenport, 1992) and smaller than those of Fish (Fish, 1990). If the fish wing had shrunk after death and its shape significantly modified (Davenport, 1992), the lift force measured from the wind tunnel experiment would be remarkably different from the body mass. However, as shown in Fig. 4, the two data (the mass and lift force) agree very well with each other, indicating that our fish models (at least L_1 and much L_3) did not shrink much.

Force and moment measurements

The lift (C_L), drag (C_D) and pitching moment (C_M) coefficients are defined as $C_L=L/(0.5\rho u^2_\infty A)$, $C_D=D/(0.5\rho u^2_\infty A)$ and $C_M=D/(0.5\rho u^2_\infty A)$, respectively, where ρ is the air density, A is the reference area ($=A_1+A_2+A_3$) for the flying-fish model, and L, D and M are the lift, drag and pitching moment, respectively. Since we measured total aerodynamic forces and moment exerted on the wings and body of flying fish, we defined the reference area as the sum of the planform areas of the pectoral (A_1) and pelvic (A_2) fins and body (A_3).

Fig. 5 shows the variations of lift (C_L) and drag (C_D) coefficients with the angle of attack (α) for models L_1–L_3, M and N. As shown in Fig. 5A, the lift coefficients for models L_1–L_3 and M are largest at α=30–35 deg. In previous studies, the flying fish was observed to emerge from the sea at α=30 deg from the horizontal surface and perform taxiing (Hertel, 1966; Davenport, 1994). Because the largest lift force is required for the flying fish to take off, the present result supports those observations assuming that the take-off angle is similar to the emerging angle of the fish from the sea. Interestingly, the lift coefficients of models L_1–L_3 and M do not fall off sharply and show broad peaks at high angles of attack with little loss of lift force even after stall. This observation agrees with the characteristics of the thin-airfoil stall suggested by McCullough and Gault (McCullough and Gault, 1951) who classified the characteristics of the airfoil stall at low Reynolds number as the trailing-edge stall, leading-edge stall and thin-airfoil stall, respectively. With the thin-airfoil stall occurring on a thin airfoil with a sharp leading edge, the lift coefficient curve is relatively flat even after stall. Since the wings of our fish models were thin and operated at low Reynolds

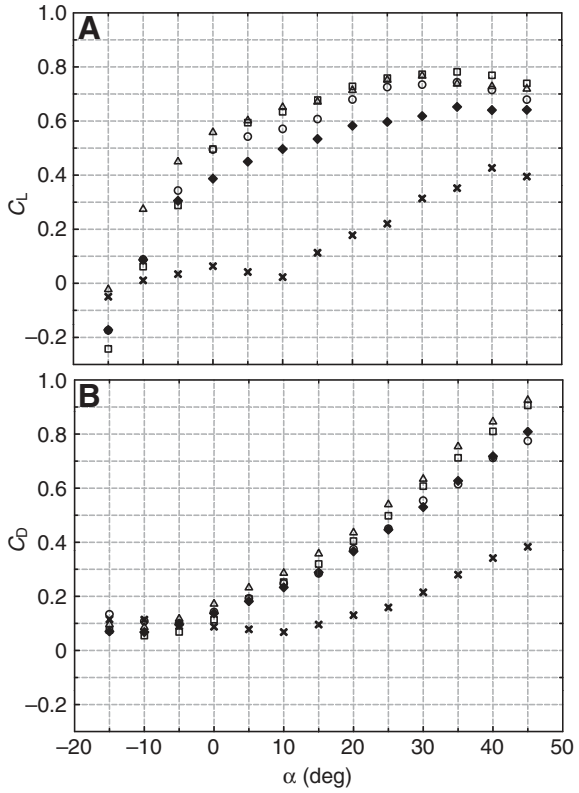

Fig. 5. Variations of the lift (C_L) and drag (C_D) coefficients with the attack angle (α). (A) C_L. (B) C_D. Open circle, Model L_1; open triangle, model L_2; open square, model L_3; closed diamond, model M; ×, model N.

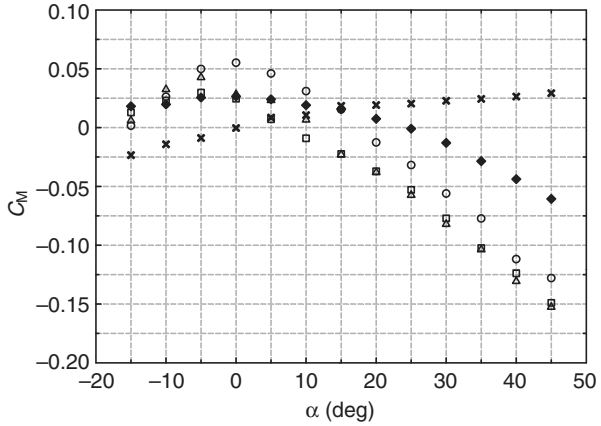

Fig. 6. Variations of the pitching moment coefficients (C_M) with the attack angle (α). Positive C_M indicates a nose-up pitching moment about the center of gravity, whereas negative C_M indicates a nose-down pitching moment. Open circle, Model L_1; open triangle, model L_2; open square, model L_3; closed diamond, model M; ×, model N.

number, they had the thin-airfoil stall characteristics. With smaller β_1 (from L_1 to L_3), the lift coefficient becomes larger at $\alpha>10$ deg, but the amount of its difference is quite small (less than 7%). However, the drag coefficients for models L_1–L_3 and M were minimum at $\alpha=-10$ deg to -5 deg and rapidly increased with increasing α (Fig. 5B). Without the enlarged pelvic fins (model M), the lift coefficient is smaller than those with pectoral and pelvic fins (models L_1–L_3) by more than 20% at $\alpha\geq0$ deg. The drag coefficient of model M is similar to or smaller than those of models L_1–L_3 by about 10% at $\alpha\geq0$ deg. Thus, the enlarged pelvic fins contribute to the generation of aerodynamic force, especially to the increase of lift force, which is attributed to the accelerated jet-like flow structure between the pectoral and pelvic fins (see below).

The variation of pitching moment coefficient (C_M) with α is shown in Fig. 6. For a glider to have a longitudinal static stability, the nose-down pitching moment should increase with increasing α (Thomas and Taylor, 2001). That is, a negative slope of the pitching moment curve ($\partial C_M/\partial\alpha<0$) is necessary for positive static stability: the more negative (steeper) the slope, the more stable the glider. In addition, a positive pitching moment (nose-up pitching moment) is necessary at the attack angle of zero lift for a balanced flight (Thomas and Taylor, 2001). As shown in Fig. 6, the slopes of the pitching moment curve were more negative for models L_1–L_3 than that for model M, indicating that the enlarged pelvic fins enhance the longitudinal static stability. Thus, the pelvic fins have a similar role to that of a tailplane. The pelvic fins of shark have also been shown to increase, to a small extent, the static stability for pitching movements (Harris, 1938). For models L_1–L_3, the slope of pitching moment coefficient curve of L_1 (having largest β_1) becomes slightly more negative than the others, so model L_1 showed slightly better longitudinal stability than models L_2 and L_3. In general, it is known that the lateral dihedral angle of the wing enhances the lateral static stability of the wing at the cost of lift (Thomas and Taylor, 2001). In our flying fish, the lateral dihedral angle also slightly enhanced the longitudinal static stability. Without both the pectoral and pelvic fins, a positive slope of the pitching moment curve was observed, indicating unstable static characteristics.

In Fig. 7, the variations of the lift-to-drag ratios (L/D) for models L_1–L_3, M and N with α are shown. For models L_1–L_3 and M, the L/Ds are maximum at $\alpha=-5$ to 0 deg, indicating that the flying fish exhibits best gliding capabilities when it glides nearly parallel to the sea surface. This also agrees with previous observations that most trajectories of flying fish are observed to be nearly parallel to the sea surface (Latimer-Needham, 1951; Hertel, 1966; Fish, 1991; Kawachi et al., 1993). At $\alpha\geq-5$ deg, the L/Ds of models L_1–L_3 are larger than that of model M, indicating that the enlarged pelvic fins increase the glide distance of the flying fish. In previous studies, it was observed that the four-winger (biplane-typed) flying fish glides longer distances than the two-winger (monoplane-typed) flying fish

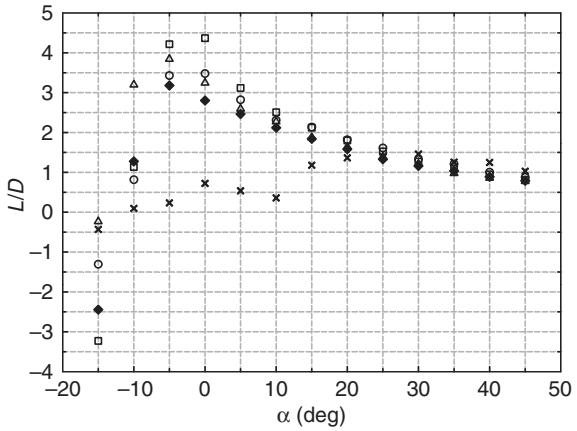

Fig. 7. Variations of the lift-to-drag ratio with the attack angle (α). Open circle, Model L_1; open triangle, model L_2; open square, model L_3; closed diamond, model M; ×, model N.

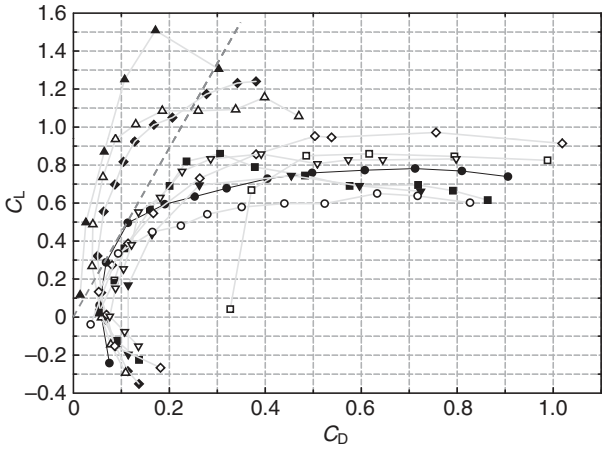

Fig. 8. Glide polars of various animal wings and a mechanical wing; closed circle, flying fish (present model L_3; α=–15 to 40 deg); open circle, swallowtail butterfly (Park et al., 2010) (α=0 to 50 deg); closed triangle, NACA 2409 (Vogel, 1967) (α=0 to 22 deg); open triangle, vulture (Vogel, 1967) (α=–20 to 16 deg); closed diamond, nighthawk (Withers, 1981) (α=–6 to 20 deg); open diamond, hawk (Withers, 1981) (α=–15 to 45 deg); closed square, petrel (Withers, 1981) (α=–12 to 45 deg); open square, fruit fly (Vogel, 1967) (α=0 to 50 deg); inverted closed triangle, bumblebee (Dudley and Ellington, 1990) (α=–10 to 50 deg); inverted open triangle, wood duck (Withers, 1981) (α=–10 to 30 deg).

(Fish, 1990; Davenport, 1992). Among models L_1–L_3, model L_3 (having the smallest β_1) has the largest value of maximum L/D. The L/Ds of models L_1–L_3 and M are larger than that of model N (body only) at $\alpha \leq 20$ deg, but are almost the same at $\alpha > 20$ deg. This indicates that the enlarged pectoral and (or) pelvic fins do provide favorable aerodynamic function at small and moderate attack angles of $\alpha \leq 20$ deg.

To compare the gliding performance of the flying fish, the glide polar (C_L *vs* C_D) of our flying fish (model L_3 showing the largest value of maximum L/D of the five models) is shown together with those of other animals' wings (when they glide) and NACA2409. The morphometric and aerodynamic properties of various wings are listed in Table 2. Note that, for other insects and birds (Fig. 8), the lift and drag forces are measured only on the wings isolated from the body. The slope of the straight line, which is tangential to the polar curve and passes through the origin, represents the maximum lift-to-drag ratio of the relevant wing (see, for example, the dashed line in Fig. 8 for the L_3 model). In terms of maximum L/D, the gliding performance of flying fish is worse than that of NACA2409, wings of nighthawk and vulture having high aspect ratios (see Table 2), but is better than that of flying insect wings (note, however, that their operating Reynolds numbers are lower than our models), and comparable to those of wings of birds such as the hawk, petrel and wood duck.

As mentioned before, the data from other animals obtained by previous researchers (in Table 2 and Fig. 8) were obtained from the measurements on the wing only. During the gliding flight of birds or insects, the body generates additional lift and drag, so one should include them for the estimation of aerodynamic performance. For gliding birds, the planform area of a bird's body is less than one-third of total planform area of wings and body (Tucker and Parrott, 1970). However, the body lift has been measured to support about 16% of the total lift force [zebra finch at gliding flight (Tobalske et al., 1999)], and the drag force on the body may not be negligible but smaller than that of the wings. Thus, we may estimate that the total $C_{L,\,MAX}$ and $C_{D,\,MIN}$ of the wings and body of gliding bird (based on the total planform area) would be slightly smaller than that of the wing only. In the case of a flying insect, the lift on the body is a small fraction (less than 10%) of the total lift, but the drag on the body is much larger than that of wing (Dudley, 2000). It follows that the total $C_{L,\,MAX}$ and $C_{D,\,MIN}$ of the body and wings of a flying insect would be smaller and larger, respectively, than those of the wing only. Thus, we may conclude that the aerodynamic performance of our flying fish is comparable to those of certain species of bird and better than those of most flying insects, even after considering the drag and lift forces on the body.

Flow structure around a gliding flying fish

Fig. 9 shows the streamwise flow structures around a flying fish (model L_3 at four different angles of attack). At the spanwise location where pectoral and pelvic fins overlap (left column), we observed an interesting flow structure. Flow goes smoothly over the pectoral and pelvic fins without separation at α=0 deg, at which the lift-to-drag ratio is maximum (Fig. 7). At α=10 deg, the flow separates at the leading edge of the pectoral fin and re-attaches on the fin forming a separation bubble. When the attack angle is larger than 10 deg, full separation occurs at the leading edge of the pectoral fin and the drag force rapidly increases with increasing α. As noted before, our flying fish model has a tandem wing configuration (bi-plane type), where the upper (pectoral fins) and lower (pelvic fins) wings were staggered and the incidence angles were 12 deg and 5 deg, respectively. Because of this configuration, at $\alpha \geq 10$ deg, there was a jet-like accelerating flow (denoted by the circles in Fig. 9B,C) at which both the pectoral and pelvic fins exist. At the spanwise

Table 2. Morphometric and aerodynamic characteristics of various animal wings

	AR	L/D_{MAX}*	$C_{L,MAX}$*	$C_{D,MIN}$*	*Re*	Reference
Flying fish† (*Cypselurus hirai*)	10.7	4.37 (0)	0.78 (35)	0.055 (–10)	2.0×10^4	Present study
Swallowtail butterfly (*Graphium policenes policenes*)	3.72	3.58 (5)	0.65 (40)	0.036 (0)	1.4×10^4	Park et al., 2010
NACA 2409	12	19.1 (5)	1.51 (19.5)	0.01 (0)	5.0×10^4	Vogel, 1967
Vulture wing (*Coragyps atratus*)	15.8	17 (5)	1.15 (12)	0.02 (0)	$O(10^4)$	Withers, 1981
Nighthawk wing (*Chordeiles minori*)	8.2	9 (6)	1.15 (15)	0.05 (3)	$O(10^4)$	Withers, 1981
Hawk wing (*Buteo lineatus*)	6.0	3.8 (6)	1.0 (25)	0.07 (2)	$O(10^4)$	Withers, 1981
Petrel wing (*Oceanodroma leucorhoa*)	8.2	4.0 (8)	0.88 (13)	0.07 (0)	$O(10^4)$	Withers, 1981
Fruit fly wing (*Drosophila virilis*)	5.5	1.8 (15)	0.87 (30)	0.33 (0)	2.0×10^3	Vogel, 1967
Bumblebee wing (*Bombus terrestris*)	6.7	2.48 (15)	0.78 (30)	0.13 (0)	1.2×10^3	Dudley and Ellington, 1990
Wood duck wing (*Aix sponsa*)	6.2	3.8 (8)	0.9 (20)	0.1 (1)	$O(10^4)$	Withers, 1981

Note that data from previous studies are based on a wing only without the body.
*Numbers inside the parentheses denote the attack angles (in degrees) at which the L/D_{MAX}, $C_{L,MAX}$ and $C_{D,MIN}$ are measured for each wing.
†Model L_3.

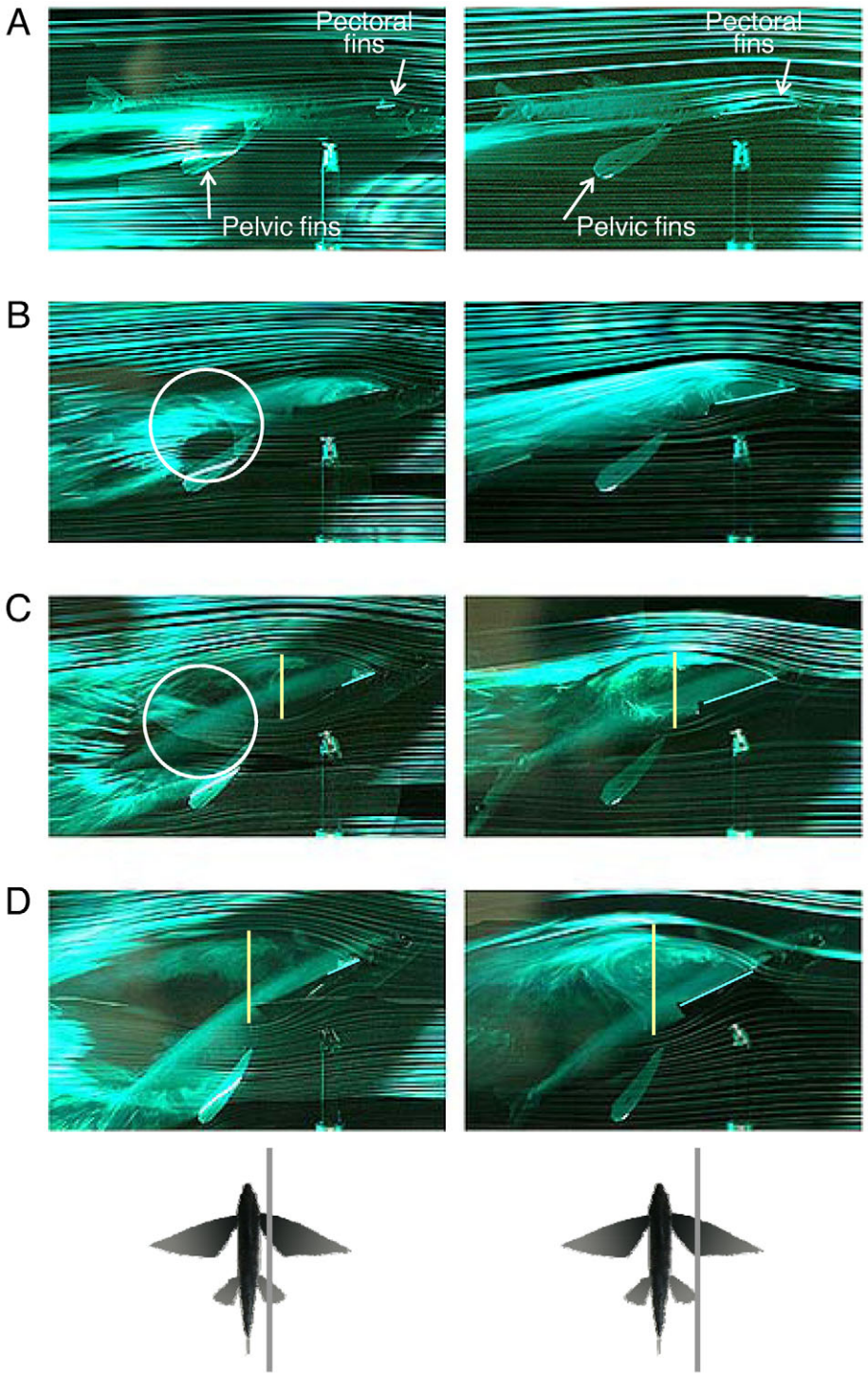

Fig. 9. Streamwise flow structure around a flying fish (model L_3) at the spanwise locations of z/S=0.1 (left) and 0.18 (right) at the attack angle of (A) 0 deg; (B) 10 deg; (C) 20 deg; (D) 30 deg. The schematic diagram in the last row illustrates the visualized spanwise locations. The flow goes from right to left.

location of the middle of the pectoral fin (right column), however, the pelvic fin does not exist. Thus, the jet-like flow structure is not observed. This jet-like flow structure accelerates the flow above the pelvic fin and thus increases its lift force as we found from force measurement (Fig. 5). Comparing the wake widths behind the pectoral fin at z/S=0.1 and 0.18, we see that the jet-like flow also reduces the wake width behind the pectoral fin (denoted by the vertical bars in Fig. 9C,D) and thus is expected to reduce the drag force exerted on the pectoral fin.

As shown, the pectoral fin of flying fish has a positive incidence angle (β_2) from the horizontal, such that wing-tip vortices are readily generated even when the flying fish glides nearly parallel to the sea surface. In addition to this, the wing of flying fish is very thin and has a pointed wing-tip shape. Consequently, strong counter-rotating wing-tip vortices exist in the wake behind a gliding flying fish even at α=0 deg (Fig. 10). This wing-tip vortex induces a downward flow in the wake, resulting in an induced drag in addition to the form and skin friction drag. For subsonic aircrafts or fighter planes operating at the Reynolds number of 10^7–10^8, the skin friction (of the wings and body) and induced drag constitute more than 90% of total drag force (Filippone, 2000). However, the contribution of

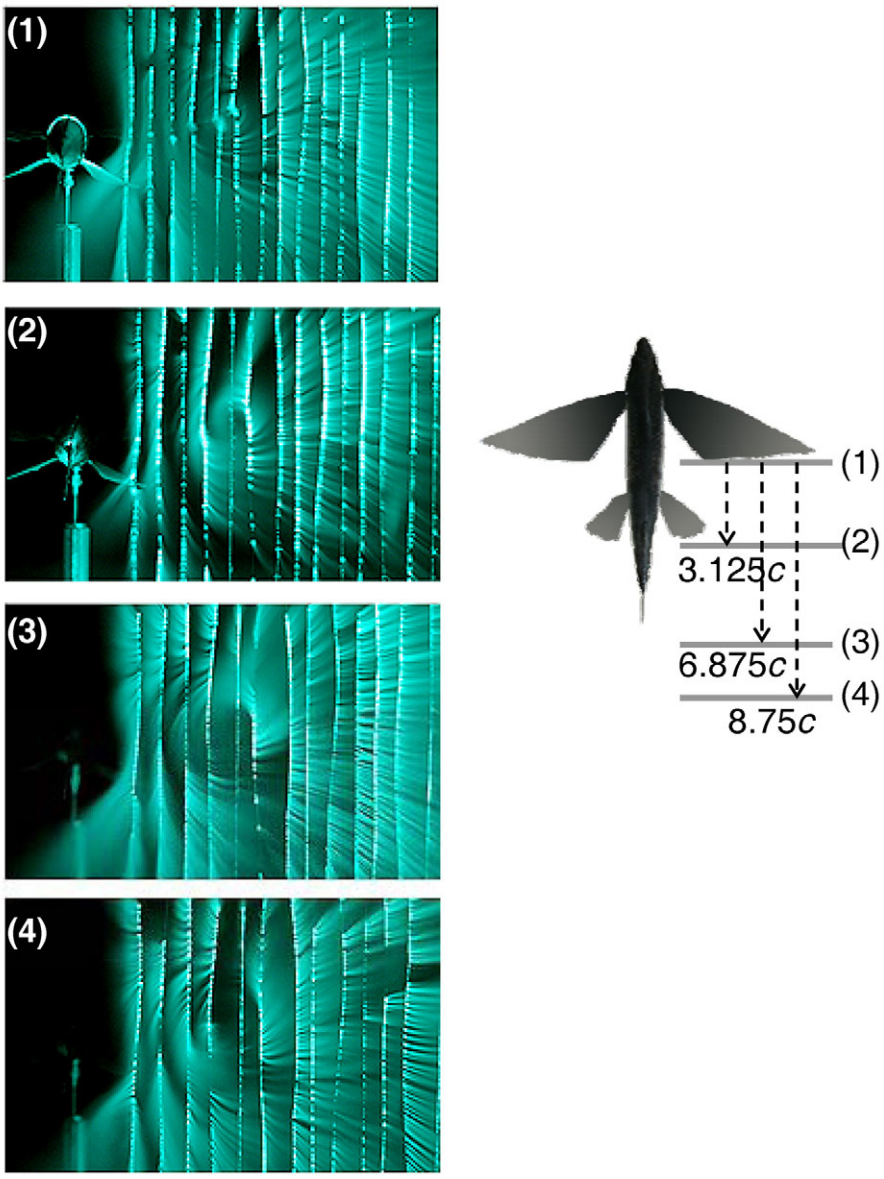

Fig. 10. Flow visualizations: end views at four streamwise locations. The schematic diagram on the right illustrates the location of the laser sheet for each visualization.

induced drag to total drag increases and that of the skin friction decreases with decreasing Reynolds number (Blake, 1983). Therefore, it seems that the induced drag is one of the dominant drag components of the gliding flying fish (Re ~10^4).

Aerodynamic properties of flying-fish body

Although the flying fish uses its hypertrophied pectoral and pelvic fins in gliding, the fins are usually folded against the body when the fish swims in the sea. In this section, we briefly investigate the aerodynamic properties of the body itself. The variations of lift, drag (Fig. 5) and pitching moment coefficients (Fig. 6) are shown for the model N (body only with both the pectoral and pelvic fins folded) with α. The lift coefficient is nearly zero at α=–10 deg and the drag coefficient is lowest at α=10 deg. Both the drag and lift coefficients rapidly increase with increasing α at α>10 deg (Fig. 5). Like almost all other fishes during swimming (Harris, 1938), the flying-fish body itself shows longitudinally unstable characteristics in the pitching direction: that is, $\partial C_M/\partial\alpha>0$ (Fig. 6). However, the flying fish with the pectoral and pelvic fins unfolded (models L_1–L_3 and M) shows statically stable characteristics.

To estimate the contribution of the flying-fish body to aerodynamic forces, we show the ratios of the drag and lift forces of model N to those of model L_3 with α in Fig. 11. Although the body shapes of two models are not exactly same, the size of the bodies are very similar to each other (see Table 1), so the contribution of the body to the aerodynamic force generation can be estimated. At $\alpha\leq$10 deg, the contribution of the body to total lift force is small (less than 7%), but increases with increasing angle of attack at α>10 deg and reaches almost 20% of total lift force at α=40 deg. However, the contribution of the body to total drag force decreases with the attack angle at α<10 deg, becomes minimum at α=10 deg, and slowly increases (from 10% to 15%) at $\alpha\geq$10 deg. Since the wing of flying fish is very thin and the incidence angle of pectoral fins of model L_3 is β_2=12 deg, the contribution of the body to total drag force is largest at α=–10 deg (about 75%).

Ground effect

It has been shown in the literature that the ground effects are different for two- and three-dimensional bodies. For a two-dimensional body, the drag force decreases when the height between the body and the

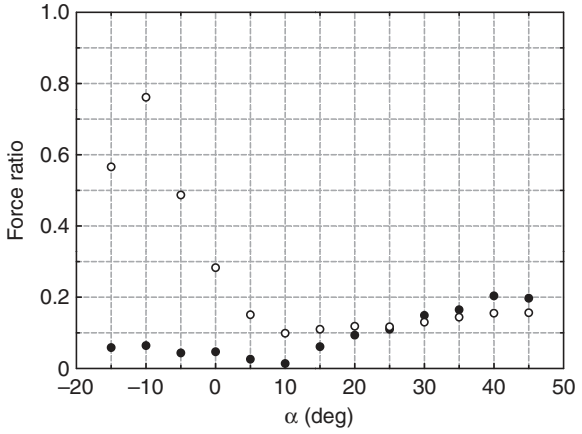

Fig. 11. Ratios of the lift and drag forces of model N to those of model L_3 with the angle of attack: closed circle, lift force; open circle, drag force.

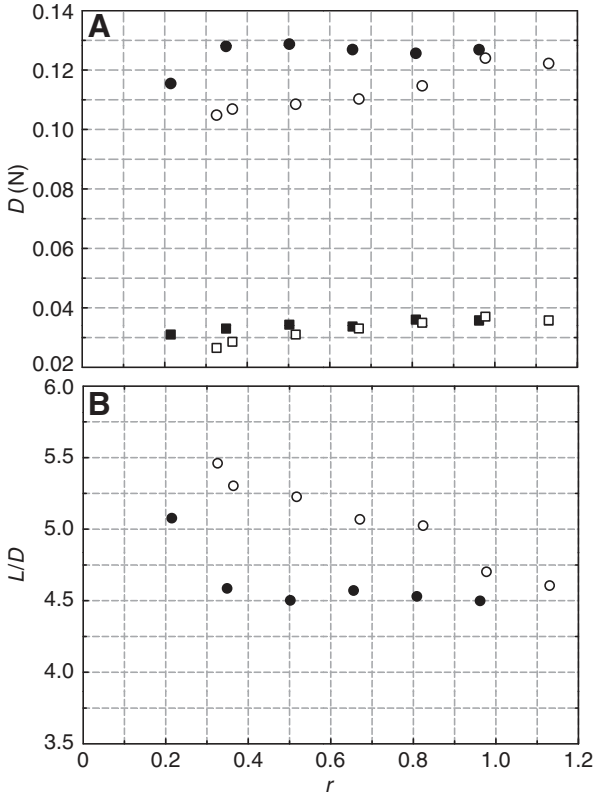

Fig. 12. Variations of the drag force and lift-to-drag ratio with the ratio (r) of flight height (h) to the half wing span (b). (A) Drag force: closed circle, model L_3 with solid surface; open circle, model L_3 with water surface; closed square, model N with solid surface; open square, model N with water surface. (B) Lift-to-drag ratio: closed circle, model L_3 with solid surface; open circle, model L_3 with water surface. Forces are measured at α=0 deg.

ground is very small (h/H ~0.2, h and H are the flight height and body height, respectively), since the ground prevents the generation of Karman vortex shedding that is the main cause of drag on a two-dimensional body (Kim and Geropp, 1998; Choi and Lee, 2000; Ahmed and Sharma, 2006). The lift force also increases with decreasing gap due to the increased pressure under the body. Unlike the two-dimensional body, a three-dimensional body under the ground effect experiences drag reduction but with nearly constant lift force (Withers and Timko, 1977; Hoerner, 1985; Sardou, 1986; Barlow et al., 2001; Zhang et al., 2004). Here, the drag reduction comes from two sources; one is the reduction of induced drag as the ground affects the movement and diffusion rate of the counter-rotating tip vortices, and the other is the reduction of form drag as the blockage effect by the ground hinders the generation of the wake vortices. By contrast, in previous studies based on a potential flow lifting-line theory (Blake, 1983; Rayner, 1991), it has been suggested that the reduction of induced drag is obtained when the ratio r (r=h/b, where b is the half wing span) is smaller than 0.5 (e.g. about 20% reduction of the induced drag at r=0.3). Since our flying-fish model has both wing and body, the ground effect should be complicated.

When they fly nearer the ground, the flyers can obtain considerable advantages in the aerodynamic performance as noted above (Blake, 1983; Rayner, 1991). It has been suggested that the flying fish takes advantage of the ground effect to prolong the gliding distance by increasing the lift-to-drag ratio, especially during take-off and end phase of the flight (Fish, 1990; Kawachi et al., 1993; Davenport, 1994; Vogel, 1994; Davenport, 2003). We installed a water surface at the bottom of the wall of the test section and investigated the effect of water surface (slip boundary) on the aerodynamic forces of a gliding flying fish (see Materials and methods). Furthermore, we considered two fish models (L_3 and N) in ground effect, i.e. with and without the fins (wing).

Fig. 12 shows the variations of drag force and lift-to-drag ratio with the ratio of the flight height (h) to the half wing span (b=S/2), r=h/b. The lift force was almost unaffected by the ground for all r values considered in this study (not shown here). The amount of drag reduction due to ground effect is larger for a water surface than for a solid surface. For model L_3, the drag force was nearly constant at r>0.35 but decreased by 9% at r=0.21 in the case of solid surface. However, the drag force with a water surface started to decrease with decreasing r from r≈0.97 and maximum reduction of the drag by 14% was obtained at r=0.33. Consequently, the lift-to-drag ratios for both solid and water surfaces increased with decreasing r from r=0.35 and 0.97, respectively (Fig. 12B). For model N (body only), drag reductions of 4% (at r=0.21) and 7% (at r=0.33) were from its body only for solid and water surfaces, respectively, whereas the of 9% and 14% were from the body and wing for model L_3. Therefore, the drag reduction by ground effect comes almost equally from the body and wing.

Since it is assumed that a significant amount of induced drag is exerted on the flying fish, we visualized the wake behind the flying fish to examine the wing-tip vortices with varying flight height. Fig. 13 shows the flow visualizations at three y–z planes for r=1.12 and 0.33 in the case of water surface. When r was small (r=0.33), the wing-tip vortex interacted with the water surface and lost its strength faster than that when r=1.12 (Zerihan and Zhang, 2003; Barber, 2007), resulting in the reduction of the induced drag. Therefore, the drag reduction on a gliding flying fish in ground effect comes from (1) the direct blockage effect between the whole body and the ground, and (2) modification of the wing-tip vortices. Considering the real situation of gliding flying fish, the slip velocity of the water surface should be u_∞–u_{ind}, where u_∞ is the flying speed of the fish and u_{ind} is the wind-induced surface velocity; u_{ind}≈0.03u_∞ (Wu, 1975; Tsanis, 1989). The experimental setup satisfying this requirement is not possible with the wind tunnel used, but we expect bigger drag reduction in the real situation than that shown in Fig. 12A.

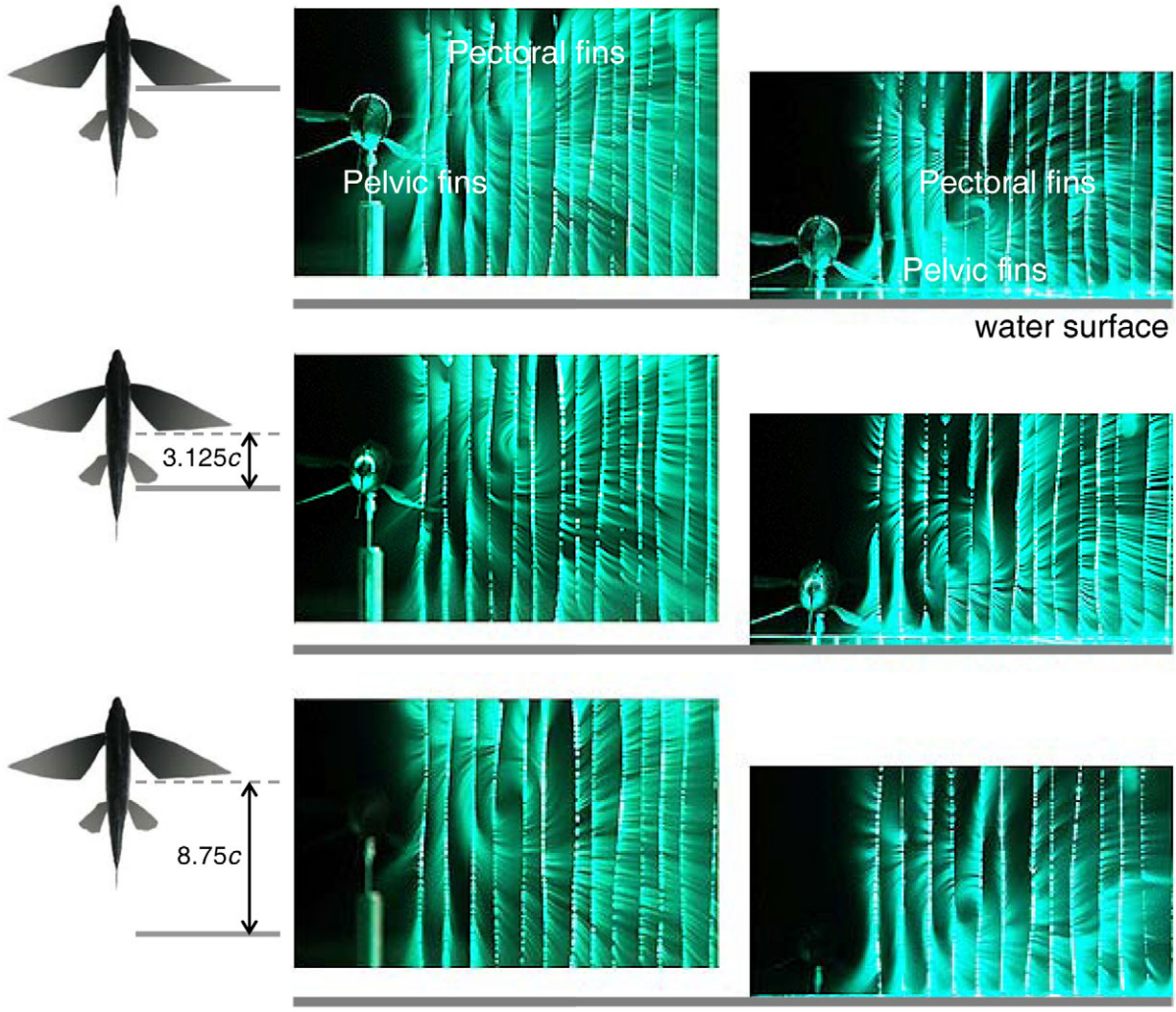

Fig. 13. Flow visualizations: end views for the case of water surface at h=1.12 (middle column) and h=0.33 (right column). The schematic diagram on the left illustrates the location of the laser sheet for each visualization.

Concluding remarks

For the first time, we have performed a direct wind-tunnel experiment to investigate the aerodynamic properties of flying-fish flight and provided qualitative and quantitative data for the flying fish flight. Force measurements were performed for the real flying-fish models with different wing morphologies. The aerodynamic performance of flying fish is comparable to those of various bird wings, and the flying fish has some morphological characteristics in common with the aerodynamically designed modern aircrafts. The maximum lift coefficient of flying fish is measured at α=30–35 deg where the flying fish is observed to emerge from the sea. The lift-to-drag ratio is largest at α=–5~0 deg, indicating that the best gliding performance can be achieved when the flying fish glides nearly parallel to the sea surface. As the lateral dihedral angle of the pectoral fins decreases, the lift coefficient slightly increases. In addition to the enlarged pectoral fins, the large pelvic fins have an important role in enhancing the lift-to-drag ratio and longitudinal static stability. The enhancement of the lift-to-drag ratio from the pelvic fin is attributed to the jet-like flow existing between the pectoral and pelvic fins. For both solid and water surfaces, the drag coefficient decreases and thus the lift-to-drag ratio increases as a result of the ground effect, indicating that the flying fish obtains substantial advantages by gliding close to the sea surface. The ground effect is more pronounced for the water surface having a slip boundary condition.

In the present study, as shown above, we examined the variations of aerodynamic force with the changes in the wing morphology, such as the angle of attack and lateral dihedral angle. The gliding performance (i.e. maximum lift-to-drag ratio) was enhanced as the lateral dihedral angle of pectoral fins decreased. However, in a few previous studies, it was observed that the flying fish glides with pronounced lateral dihedral angle of the pectoral fins (Hubbs, 1933; Fish, 1990; Davenport, 1994). Hubbs (Hubbs, 1933) argued that the flying fish controls the aerodynamic forces by varying the dihedral and attack angles of the pectoral fins. It is known that the positive wing dihedral angle provides rolling stability to restore the glider to the level flight (Thomas and Taylor, 2001). This positive lateral dihedral angle reduces the effective span of the wing, thus reducing the lift force. Thus, in the future it would be interesting to investigate the trade-off between the rolling stability and the lift-to-drag ratio with the lateral dihedral angle.

Finally, it has been argued that the flying fish has the ability to change the camber as well as the angle of attack and dihedral angle of the wings, although the specific variation of the camber during

its flight is not known (Breder, 1930; Hubbs, 1933). Similar to a previous study (Davenport, 1994), the present flying fish models have slightly cambered pectoral fins and flat pelvic fins. In general, the camber is known to increase the lift force at least for low angles of attack. Therefore, the role of camber on the forces on the wing during the flight of flying fish should be another interesting topic to pursue in the future.

ACKNOWLEDGEMENTS

Preliminary results of this work were presented at the IUTAM Symposium on Unsteady Separated Flows and Their Control, Corfu Island, Greece, June 18-22, 2007, and published in the Proceedings of this symposium (Park and Choi, 2009). We appreciate the cooperation from the National Federation of Fisheries Cooperatives of Korea and the Korea Research Center of Maritime Animals for preparing the flying-fish models. We also thank Dr Woo-Pyung Jeon for the help in the initial setup of our experiment. This work was supported by a National Research Laboratory Program (R0A-2006-000-10180-0), a World Class University Program (R31-2008-000-10083-0), and a Converging Research Center Program (2009-0082824) through the National Research Foundation of Korea funded by the Ministry of Education, Science, and Technology, Korea.

LIST OF SYMBOLS

A	total planform area ($=A_1 + A_2 + A_3$)
A_1	planform area of pectoral fins
A_2	planform area of pelvic fins
A_3	planform area of body
AR	aspect ratio ($=S^2/A_1$)
b	half wing span ($=S/2$)
c	average chord length of pectoral fins ($=A_1/S$)
C_D	drag coefficient
C_L	lift coefficient
C_M	pitching moment coefficient
D	drag force
h	flight height (distance between the ground and the lower surface of the body)
L	lift force
L/D	lift-to-drag ratio
M	pitching moment
r	ratio of flight height to half wing span ($=h/b$)
Re	Reynolds number ($=uc_\infty/\nu$)
S	wing span of pectoral fins
SL	standard length
u_{ind}	wind-induced water velocity
u_∞	freestream velocity
x_{CG}	location of the center of gravity
α	angle of attack
β_1	lateral dihedral angle of pectoral fins
β_2	incidence angle of pectoral fins
β_3	incidence angle of pelvic fins
υ	kinematic viscosity

REFERENCES

Ahmed, M. R. and Sharma, S. D. (2006). An investigation on the aerodynamics of a symmetrical airfoil in ground effect. *Exp. Therm. Fluid. Sci.* **29**, 633-647.
Barlow, J. B., Guterres, R. and Razenbach, R. (2001). Experimental parametric study of rectangular bodies with radiused edges in ground effect. *J. Wind Eng. Ind. Aerodyn.* **89**, 1291-1309.
Barber, T. J. (2007). A study of water surface deformation due to tip vortices of a wing-in-ground effect. *J. Ship Res.* **51**, 182-186.
Blake, R. W. (1983). Mechanics of gliding in birds with special reference to the influence of the ground effect. *J. Biomech.* **16**, 649-654.
Breder, C. M., Jr (1930). On the structural specialization of flying fishes from the standpoint of aerodynamics. *Copeia* **4**, 114-121.
Choi, J.-H. and Lee, S.-J. (2000). Ground effect of flow around an elliptic cylinder in a turbulent boundary layer. *J. Fluid Struct.* **14**, 697-709.
Davenport, J. (1992). Wing-loading, stability and morphometric relationships in flying fish (exocoetidae) from the north-eastern atlantic. *J. Mar. Biol. Assoc. UK* **72**, 25-39.
Davenport, J. (1994). How and why do flying fish fly? *Rev. Fish Biol. Fish.* **40**, 184-214.
Davenport, J. (2003). Allometric constraints on stability and maximum size in flying fishes: implications for their evolution. *J. Fish Biol.* **62**, 455-463.
Dudley, R. (2000). *The Biomechanics of Insect Flight*. Princeton, NJ: Princeton University Press.
Dudley, R. and Ellington, C. P. (1990). Mechanics of forward flight in bumblebees II. Quasi-steady lift and power requirements. *J. Exp. Biol.* **148**, 53-88.
Filippone, A. (2000). Data and performances of selected aircraft and rotorcraft. *Prog. Aerosp. Sci.* **36**, 629-654.
Fish, F. E. (1990). Wing design and scaling of flying fish with regard to flight performance. *J. Zool. Lond.* **221**, 391-403.
Fish, F. E. (1991). On a fin and a prayer. *Scholars* **3**, 4-7.
Harris, J. E. (1938). The role of the fins in the equilibrium of the swimming fish II. The role of the pelvic fins. *J. Exp. Biol.* **15**, 32-47.
Hertel, H. (1966). Take-off and flight of the flying fish. In *Structure-Form-Movement* (ed. M. S. Katz), pp. 218-224. New York: Reinhold Publishing Company.
Hoerner, S. F. (1985). *Fluid-dynamic Lift*. Princeton, NJ: Princeton University Press.
Hubbs, C. L. (1933). Observations on the flight of fishes, with a statistical study of the flight of the Cypselurinae and remarks on the evolution of the flight of fishes. *Pap. Mich. Acad. Sci.* **17**, 575-611.
Kawachi, K., Inada, Y. and Azuma, A. (1993). Optimal flight path of flying fish. *J. Theor. Biol.* **163**, 145-159.
Kim, M. S. and Geropp, D. (1998). Experimental investigation of the ground effect on the flow around some two-dimensional bluff bodies with moving-belt technique. *J. Wind Eng.* **74**, 511-519.
Latimer-Needham, C. H. (1951). Flying-fish aerodynamics. *Flight* **26**, 535-536.
McCullough, G. B. and Gault, D. E. (1951). Examples of three representative types of airfoil-section stall at low speed. *NACA TN*-2502.
Mills, C. A. (1936a). Source of propulsive power used by flying fish. *Science* **83**, 80.
Mills, C. A. (1936b). Propulsive power used by flying fish. *Science* **83**, 262.
Park, H. and Choi, H. (2009). Investigation of aerodynamic capabilities of flying fish in gliding flight. In *IUTAM Symposium on Unsteady Separated Flows and their Control* (ed. M. Braza and K. Hourigan), pp. 27-33. Dordrecht: Springer.
Park, H., Bae, K., Lee, B., Jeon, W.-P. and Choi, H. (2010). Aerodynamic performance of a gliding swallowtail butterfly wing model. *Exp. Mech.* Epub ahead of print, doi:10.1007/s11340-009-9330-x.
Rayner, J. M. V. (1986). Pleuston: animals which move in water and air. *Endeavour* **10**, 58-64.
Rayner, J. M. V. (1991). On the aerodynamics of animal flight in ground effect. *Philos. Trans. R. Soc. Lond. B. Biol. Sci.* **334**, 119-128.
Sardou, M. (1986). Reynolds effect and moving ground effect tested in a quarter scale wind tunnel over a high speed moving belt. *J. Wind Eng. Ind. Aerodyn.* **22**, 245-270.
Thomas, A. L. R. and Taylor, G. K. (2001). Animal flight dynamics I. stability in gliding flight. *J. Theor. Biol.* **212**, 399-424.
Tobalske, B. W., Peacock, W. L. and Dial, K. P. (1999). Kinematics of flap-bounding flight in zebra finch over a wide range of speeds. *J. Exp. Biol.* **202**, 1725-1739.
Tsanis, I. K. (1989). Simulation of wind-induced water currents. *J. Hydr. Eng.* **115**, 1113-1134.
Tucker, V. A. and Parrott, G. C. (1970). Aerodynamics of gliding flight in a falcon and other birds. *J. Exp. Biol.* **52**, 345-367.
Vogel, S. (1967). Flight in drosophila III. aerodynamic characteristics of fly wings and wing models. *J. Exp. Biol.* **46**, 431-443.
Vogel, S. (1994). *Life in Moving Fluids*. Princeton, NJ: Princeton University Press.
Withers, P. C. (1981). An aerodynamic analysis of bird wings as fixed aerofoils. *J. Exp. Biol.* **90**, 143-162.
Withers, P. C. and Timko, P. L. (1977). The significance of ground effect to the aerodynamic cost of flight and energetics of the black skimmer (*Rhyncops nigra*). *J. Exp. Biol.* **70**, 13-26.
Wu, J. (1975). Wind-induced drift currents. *J. Fluid. Mech.* **68**, 49-70.
Zerihan, J. and Zhang, J. (2003). Off-surface measurements of a wing in ground effect. *J. Aircraft* **40**, 716-725.
Zhang, X., Senior, A. and Ruhrmann, A. (2004). Vortices behind a bluff body with an upswept aft section in ground effect. *Int. J. Heat Fluid Flow* **25**, 1-9.